Toward an Improved Understanding of Thruster Dynamics for Underwater Vehicles

A. J. Healey, S. M. Rock, S. Cody, D. Miles, and J. P. Brown

Abstract—This paper proposes a novel approach to modeling the four quadrant dynamic response of thrusters as used for the motion control of ROV and AUV underwater vehicles. The significance is that these vehicles are small in size and respond quickly to commands. Precision in motion control will require further understanding of thruster performance than is currently available. The model includes a four quadrant mapping of the propeller blades lift and drag forces and is coupled with motor and fluid system dynamics. A series of experiments is described for both long and short period triangular, as well as square wave inputs. The model is compared favorably with experimental data for a variety of differing conditions and predicts that force overshoots are observed under conditions of rapid command changes. Use of the model will improve the control of dynamic thrust on these vehicles.

NOMENCLATURE

R	Propeller radius, m.
T	Thrust force, Newtons (N).
Q	Propeller torque, Nm.
ω_m	Motor rotational rate, rad/s.
ω_p	Propeller Rotational Rate, rad/s.
N	Reduction gear ratio.
n	Propeller revolutions per s.
L	Tunnel length, m.
D	Propeller diameter, m.
$Lift$	Lift force, N.
$Drag$	Drag force, N.
θ	Angle of inlet to blades, rad.
α_e	Effective angle of attack, rad.
p	Blade pitch, rad.
γ	Effective added mass ratio.
$\Delta\beta$	Momentum coefficient.
ρ	Mass density of water, kg/m^3.
U_a	Section average flow velocity, m/s.
U_p	Propeller velocity, m/s.
A	Tunnel cross-sectional area, m^2.
U_0	Vehicle velocity, m/s.

I. INTRODUCTION

As the use of remotely operated underwater vehicles becomes more widespread and their tasking more complex in deeper waters, there is a need to free the vehicle from the power and signal tether, and to increase both the level of control autonomy and the maneuvering precision of these underwater robots. In a recent paper, Yoerger

et al point out that underwater vehicle thrusters must be properly modeled if good results are to be obtained for the vehicle motion control. Thrusters are comprised of propellers driven by a motor—the usual way in which ships have been propelled through the seaway since the days of commercial sailing ships. However, while there is a long history of theoretical research, experimental validation and practical experiential knowledge concerning the performance of ships propellers, the issues relating to the control of remotely operated vehicles (ROV's) and autonomous underwater vehicles (AUV'S) are new because these vehicles are small, with relatively fast response, and have to execute dynamic positioning maneuvers. Within this scenario, propeller operation occurs over the full four quadrant range of the thrust/speed map.

Yoerger *et al.* [1] developed a lumped parameter model of the dynamic response of an ROV thruster that went beyond the popular notion that, for a given unit with fixed pitch blading, thrust and input torque are related to the modified square of the propeller rotational rate and the angle of advance.

They introduced the idea that fluid momentum considerations in the thruster shrouding area gives rise to a time lag in the response of thrust to stepwise inputs of motor torque. Experimental results under steady state conditions for single quadrant operation certainly verified the well known square law relationship between thrust and propeller rotational speed, and it did appear that the thrust response had long lag times at low thrust levels. However, little details were provided of the actual experimental thrust data under varied experimental conditions. For instance, dynamic energy balance arguments were applied but dynamic momentum arguments were ignored in the formulation of the thrust equation. Also, an instantaneous relationship between propeller rotational rate and the lumped parameter measure of flowrate was used which cannot be supported in reality.

We believe that such a model is still insufficient to understand the dynamic behavior of thrusters for future *high performance* underwater robotics applications. The main point of this paper then is to provide a generic thruster model that considers propeller thrust and torque as a mapping linked to lift/drag force variation with changes in the local effective angle of attack between fluid and blade—as is usual in propeller theory: also, to associate the lags and overshoots in the thrust response to lags in the development of the local angle of attack at the propeller blading and possibly to lags in the dynamic development of the blading pressure distributions. Lags in the local angle of attack apparent at the propeller blades arise because of fluid inertial factors in the shrouding around the thruster, and, for open bladed propellers, through the conversion of angular to linear momentum. Lags in the dynamic development of blade pressure distributions are a well known phenomenon.

Experimental results are provided herein that show the response of a tunnel thruster to triangular and square wave inputs at various levels of thrust. Results on an open bladed propeller also show the similar tendency that thrust response exhibits an overshoot to stepwise inputs—in contrast to the lagging response seen by Yoerger. With the relatively rapid response capable of high torque motors we claim that these more precise models will allow for better control of thrust and hence vehicle motion. Identification of a simple representation of a thrust/torque map using drag and lift coefficients is shown to provide excellent agreement in thrust response as compared to experimental data.

This paper follows from work done at MBARI, the Naval Postgraduate School and the Stanford Aerospace Robotics Laboratory in

Report Documentation Page

Form Approved
OMB No. 0704-0188

1. REPORT DATE **MAR 1995**	2. REPORT TYPE	3. DATES COVERED **00-00-1995 to 00-00-1995**

4. TITLE AND SUBTITLE	5a. CONTRACT NUMBER
Toward an Improved Understanding of Thruster Dynamics for Underwater Vehicles	5b. GRANT NUMBER
	5c. PROGRAM ELEMENT NUMBER
6. AUTHOR(S)	5d. PROJECT NUMBER
	5e. TASK NUMBER
	5f. WORK UNIT NUMBER

7. PERFORMING ORGANIZATION NAME(S) AND ADDRESS(ES) **Naval Postgraduate School ,Department of Mechanical Engineering,Monterey,CA,93943**	8. PERFORMING ORGANIZATION REPORT NUMBER

9. SPONSORING/MONITORING AGENCY NAME(S) AND ADDRESS(ES)	10. SPONSOR/MONITOR'S ACRONYM(S)
	11. SPONSOR/MONITOR'S REPORT NUMBER(S)

12. DISTRIBUTION/AVAILABILITY STATEMENT
Approved for public release; distribution unlimited

13. SUPPLEMENTARY NOTES

14. ABSTRACT
see report

15. SUBJECT TERMS

16. SECURITY CLASSIFICATION OF:			17. LIMITATION OF ABSTRACT	18. NUMBER OF PAGES	19a. NAME OF RESPONSIBLE PERSON
a. REPORT **unclassified**	b. ABSTRACT **unclassified**	c. THIS PAGE **unclassified**	**Same as Report (SAR)**	**8**	

Standard Form 298 (Rev. 8-98)
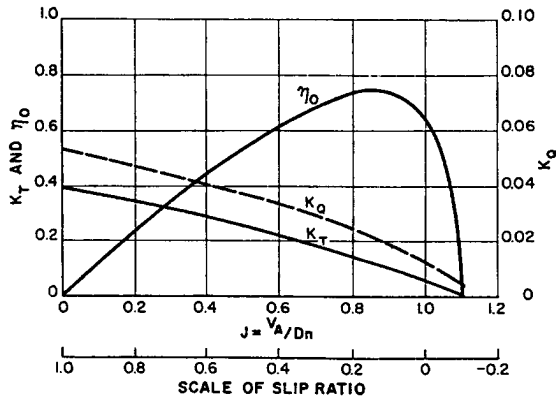Prescribed by ANSI Std Z39-18

Fig. 1. Thrust and torque coefficients versus angle of advance (Lewis [9]).

the development of the model and the experimental characterization of tunnel and open bladed thrusters [2]–[6].

II. BACKGROUND

The momentum theory of propellers developed originally by Rankine and Froude (see [7]) showed that for a propeller actuator disc, thrust can be expected to depend on the square of the flow velocity through the blading and that the energy efficiency of the propeller is increased when the thrust loading on the blade is reduced. The theory lacks detail particularly in showing how the thrust was related to the shaping of the propeller blade. Blade element theories followed that are rooted in the theory of aerodynamics (see [8]) in which the lift and drag forces generated from any element of the blade's cross section are added over the total length of the blade. The lift and drag forces are related to the local angle of attack at that blade section. A representation of the lift and drag coefficients as a function of effective angle of attack is then required in order to complete the calculation of total thrust and torque. Lift and drag coefficients are readily available for many diverse wing sections for small angles of attack and blade element theory is now widely used in the design of propellers. A full discussion of many considerations appears in Lewis, [7]. However, coefficient data for angles of attack that are larger than that which would cause stall to occur and transient response data are very scarce. Certainly, full four-quadrant data are not readily available requiring many assumptions to be made if full reversals of flow are to be modeled.

General difficulties in modeling have led to the use of simplified thrust and torque coefficients for any given propeller which are experimentally related to the speed of advance of the propeller (a measure of angle of attack) in non dimensional form as in Lewis [9] Fig. 1. The coefficients and speed of advance are defined by

$$C_T = \frac{T}{\rho n^2 D^4} \quad C_Q = \frac{Q}{\rho n^2 D^5} \quad J = \frac{U_a}{nD}.$$

These diagrams illustrate that thrust generally falls when the propeller is advanced through the water. The advance coefficient really becomes a measure of the tangent of the apparent angle of attack of water particles on the propeller blading. For propellers of differing pitch, the point at which maximum efficiency is reached depends on the coefficient of advance. Again, little data is available concerning full four quadrant operation although it is quite standard that first quadrant data is available and used routinely in the assessment of propeller behavior. Models of these static relationships were used by Fossen [10] and Sagatun [11] recently in their modeling of ROV thrusters.
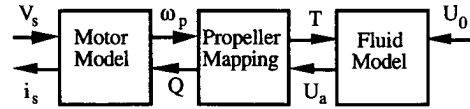

Fig. 2. Major elements of the model.

Under rapid transient conditions, we assert that it is not adequate to make the steady state assumption that

$$T \propto \omega_p |\omega_p|.$$

The four-quadrant operation of thrusters was addressed several years ago when more accurate ships' maneuvering models were sought. This led to extensive research embodied in the work of Van Lammeren et al. [12] with the Wageningen B-Series propellers operating under steady state conditions but in all four quadrants of the advance velocity/rotational velocity diagram. The results were given in terms of nondimensionalized coefficients of propeller thrust and torque as a function of the apparent angle of approach of water particles into the blades rather than local angle of attack. The four-quadrant data however were fitted with Fourier series of 10 and 20 terms so that others could numerically replicate the coefficients as part of a simulation model. The simulation of crash back and thrust reversal was addressed during those times, although surface ships, because of their large physical mass respond so slowly compared to the propulsion system that dynamic effects of thrust were found to be insignificant.

While useful, as background, we have found that these data cannot be used directly as they only relate to the Wageningen Series B blade design. And, although we could possibly generate equivalent data for each propeller used, the data required would be elaborate and specific only to the propeller tested.

III. PROPOSED MODEL

To keep the proposed model at a simple level, we can utilize well known aerofoil lift and drag data together with some interconnecting assumptions for their four-quadrant extensions similar to that used in Rickards [13] to formulate thrust and torque equations. The result is a mapping involving a number of parameters adequate for representing the four-quadrant behavior of AUV thrusters. In an ideal case, these can be established using rational engineering assumptions. Also, balancing the needs for precision with the needs for a reasonable abstraction of the physical principles, a minimum rational model for this mapping is required. The remaining key feature of the model considers the lags resulting from kinetic energy storage in the fluid medium surrounding the blades and its influence on the local effective angle of attack. The model illustrates the internal feedback structure apparent in the fluid/structure/motor interaction problem and will be shown to give reasonable agreement with experimental responses. In its generalized form the structure of the model is given in Fig. 2.

A. Motor Modeling

The motor model is standard in electromechanical modeling and is based here on a dc servo-motor permanent magnet type as in a Pitman PITMO Model 14202 dc motor driven from a voltage source as in an Analog Devices PWM control card, model 30A8DD. Voltage signals to the card convert the motor voltage to an appropriate PWM signal chopped at 35 KHz. with the dc level variable between ±23 V. The motor has a stall torque of 106 oz/in, a no load speed of 3820 r/min, and a peak power rating of 333 W. With a 2 : 1 reduction gear to drive the propeller, a 4-blade Kaplan propeller of 0.0762 m with
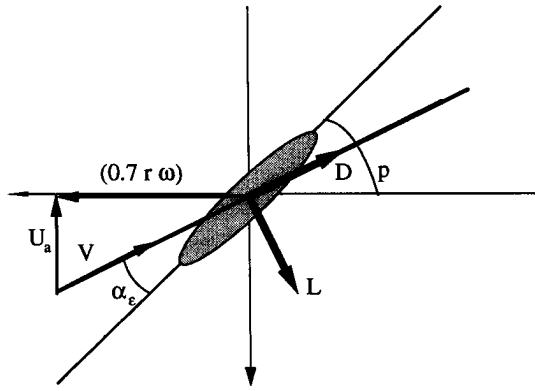
Fig. 3.   Angle of attack diagram for propeller blade.

fixed pitch at either at 45 or 30°, the linear dynamics model becomes

$$\dot{\omega}_m = -K_1\omega_m + K_2 V_s - K_h Q \tag{1}$$

$$\omega_p = \omega_m/N. \tag{2}$$

Numerical values for the parameters, K_1 and K_2 are taken from the motor characteristics that are assumed to be linear, although that is not a restriction to the fundamental concepts of the model. The parameter K_h relates to the motor deceleration from propeller hydrodynamic torque loading. The total rotational inertia includes all mechanical inertia including motor, gears and propeller. K_1 contains all viscous friction components as well as the motor characteristic resistance that gives effective damping to the motor response. In this first order model, motor field and armature inductance are neglected, so are stiction effects from nonlinear friction torque. The input to this model is a voltage source and the current draw would be an output. To model current driven motors, a simple rearrangement of the equation would be performed. The primary state variable for the motor model, however, is still its rotational rate, ω_m, and the loading is still through the propeller hydrodynamic torque load.

B. Propeller Map

The reduction gear directly connects the motor to the propeller, and for any particular blade, its tangential speed measured at some convenient radial position (usually taken at $0.7R$), is such that the tangential velocity of the fluid relative to the blade is given by,

$$U_p = 0.7R\omega_m/N. \tag{3}$$

Now, depending on the velocity of the incoming fluid particles relative to the propeller blading, U_a, an inlet effective angle of attack is established, modeled by the variable, α_e as in Fig. 3 where

$$\alpha_e = (\pi/2 - p) - \arctan\left(\frac{U_a}{U_p}\right). \tag{4}$$

The total relative velocity squared magnitude is then

$$V^2 = U_p^2 + U_a^2.$$

According to both theory and experiment in aerodynamics, the blades develop a lift force and a drag force where the lift is the component force perpendicular to the instantaneous line of action of the flow impinging on the blade. The drag force is in line with the flow. Both are related to the squared magnitude of the relative incoming flow velocity and depend on the effective angle of attack. For small angles, the lift force is linear with α_e, while the drag force is modeled better by $\alpha_e|\alpha_e|$. In our case, we need a representation over all four quadrants of α_e, as in Van Lammeran, but, to simplify to the fundamental components of their Fourier representation, we propose
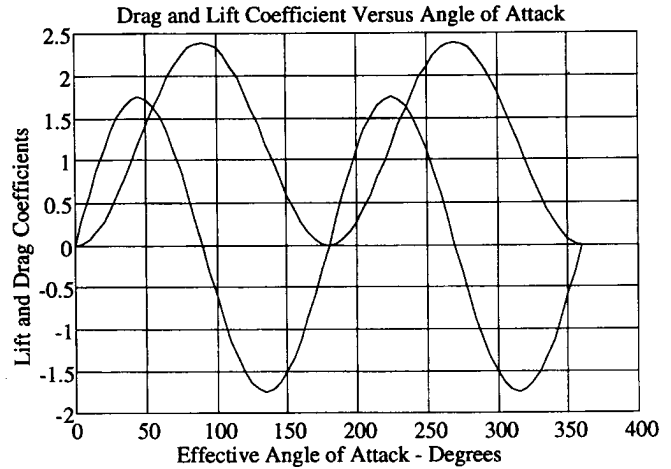

Fig. 4.   Proposed lift and drag force coefficients versus angle of attack.

initially that a formulation such as given in Fig. 4 be used. The simple harmonic form of Fig. 4 leaves only two disposable parameters, the maximum values of lift and drag coefficients, $C_{L\max}$ and $C_{D\max}$. The resulting model for the lift and drag forces on the blades is now,

$$\text{Lift} = 0.5\rho V^2 A C_{L\max}\sin(2\alpha_e) \tag{5}$$

$$\text{Drag} = 0.5\rho V^2 A C_{D\max}(1 - \cos(2\alpha_e)). \tag{6}$$

Since the lift and drag force definitions are in relation to the impinging line of flow, there is a rotational transformation required to compute the axial thrust force and the tangential force responsible for effecting the hydrodynamic loading torque. The effective radius at which the tangential force acts is $0.7R$.

$$T = \text{Lift}(\cos\theta) - \text{Drag}(\sin\theta) \tag{7}$$

$$Q = 0.7R[\text{Lift}(\sin\theta) + \text{Drag}(\cos\theta)] \tag{8}$$

where

$$\theta = p - \alpha_e.$$

C. Fluid Modeling

The connection between the motor model, and the propeller mapping model comes from the fact that as propeller rotational rate changes, so does the axial velocity through the blades. Depending on whether the blades are open or shrouded or inside a tunnel, there will be some lags in the development of changes in the axial component of flow. Also, as the thruster unit is advanced through the surrounding water, some effect on the inlet flow to the blades occurs. This area of the model concerns the fluid model.

As is usual, we apply the momentum equation to a control volume surrounding the inlet flow. For tunnel thrusters as studied by Cody [3] and McLean [2], we can relate the axial thrust to the rate of change of momentum through the control volume and,

$$T = (\rho A L\gamma)\dot{U}_a + (\rho A\Delta\beta)\overline{U}_a|\overline{U}_a|. \tag{9}$$

The term $\Delta\beta$ is a differential steady momentum flux coefficient between inlet and outlet of the control volumes on either side of the thruster unit and can only be found by experiment but range from 0.2–2.0 (see [14]). Expressing the coefficients in the above, as K_3 and K_4,

$$\dot{U}_a = -K_4 K_3^{-1}\overline{U}_a|\overline{U}_a| + K_3^{-1}T \tag{10}$$

where

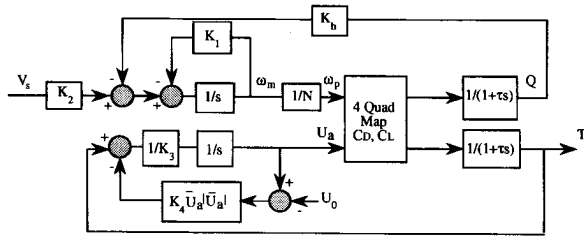$$K_3 = \rho A L\gamma, \quad K_4 = \rho A\Delta\beta \tag{11}$$

Fig. 5. System block diagram.

and

$$\overline{U}_a = (U_a - U_0). \tag{12}$$

Equation (10) represents a state equation with the primary state U_a modeling the axial flow development lags. Other lags can be identified in the development of swirl—particularly for open bladed propellers—arising from changes in *angular momentum* into the blades, but will not be elaborated further here.

IV. OVERALL MODEL SUMMARY

A system block diagram that combines the three components discussed above is presented in Fig. 5. The major contribution of this model is that it includes two state variables rather than just one. In particular, the two state variables are motor shaft speed and water velocity. Previous models used only motor shaft speed as a state, and then invoked the assumption that water velocity was directly proportional to propeller speed with the result that the slip angle was constant. Our new two-state model allows for a varying slip angle.

As described in the sections above, the motor component of this model is described by parameters K_2, K_h, and K_1. K_2 is a conversion constant that relates voltage (or current) input to torque generated in the motor. K_1 represents the motor shaft acceleration that results from internal friction in the motor (including back EMF in a voltage driven configuration). K_h relates the affect of the load torque (generated by the propeller) on motor acceleration. K_h is approximately the inverse of the effective motor shaft inertia.

The fluid component of the model is described by parameters K_3 and K_4. K_3 is roughly the apparent mass of the water that is accelerated by the propeller. K_4 describes the decelerating affects of quadratic drag on the water column.

The propeller model is represented by a four quadrant map that has been characterized simply by the parameters $C_{L\,max}$ and $C_{D\,max}$.

Finally, the time constant τ describes the axial flow development lags that result from the conversion of angular to linear momentum. This term is required when modeling open-bladed thrusters, but not tunnel thrusters.

In summary, the system state equations are

$$\dot{\omega}_m = g_1(\omega_m, U_a, V_s) \tag{13}$$

$$\dot{U}_a = g_2(\omega_m, U_a) \tag{14}$$

and the output equation for thrust is

$$T = h(\omega_m, U_a). \tag{15}$$

V. EXPERIMENTAL VALIDATION

To validate the model, experiments have been conducted on an isolated tunnel thruster unit, and an open-bladed unit. The "tunnel thruster" incorporated a high solidity propeller in a relatively long duct. The "open-bladed" unit incorporated a lower solidity propeller in a very short duct.
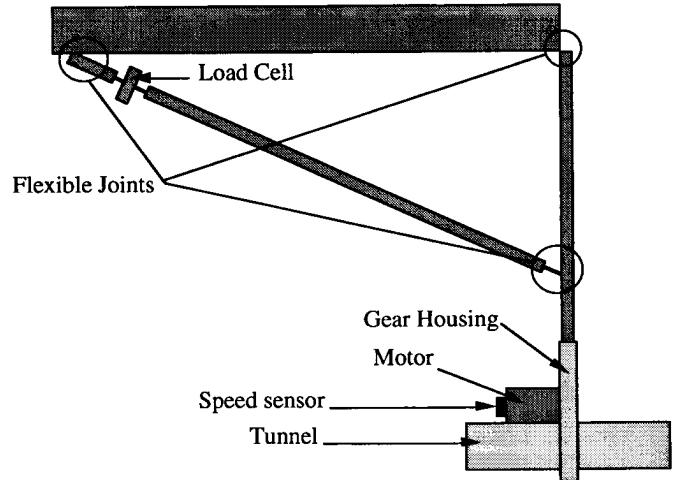

Fig. 6. Outline of thruster test stand in [3].

For both experiments a test stand was constructed that was designed to eliminate structural resonances (first structural mode was at 25 Hz) while providing clean signals representing net thrust from the unit. A schematic diagram of the test stand in presented in Fig. 6, and detailed design information is provided in [3].

VI. TUNNEL THRUSTER TESTS

A series of dynamic thrust measurements were made using the tunnel thruster. These included long, medium and short period triangular wave inputs as well as square wave inputs of voltage command covering a range of input levels.

Measurements made included motor voltage command, motor current, motor rotational speed, and net thrust. All measurements were dynamic and sampled at rates between 50 and 160 Hz depending on requirements. Sharp cutoff anti-aliasing filters were applied to each channel equally with the exception of the motor rotational speed channel which provided a clean signal from an HP optical encoder with 3000 pulses per revolution.

Blade pitch of 30° and 45° were used, and tunnel lengths of 0.419 m and 0.262 m were studied for each experimental input wave form. A table of values for the mechanical system are given in the Appendix.

The complete set of experimental data including current measurements are given in [3] to which the reader is referred for more information.

A. Long Period Triangular Wave Inputs

The benefit of a long period triangular wave input is to provide steady state results for both forward and reverse thrust commands. Fig. 7 shows the results for thrust and motor speed versus time for a 50-s period triangular wave input of command voltage to the motor. Fig. 8 converts the data into the steady state map of thrust versus speed for the tunnel thruster unit.

This data conform as expected to the notion that the thrust is proportional to the square of the propeller speed. Motor speed and voltage input are strongly related so it is not surprising that the square law relationship applies closely to the voltage/thrust behavior with a minor modification to account for motor loading effects at higher speeds. Data from these experiments confirms the thrust capability of the unit—in this case low but consistent with others results when normalized.
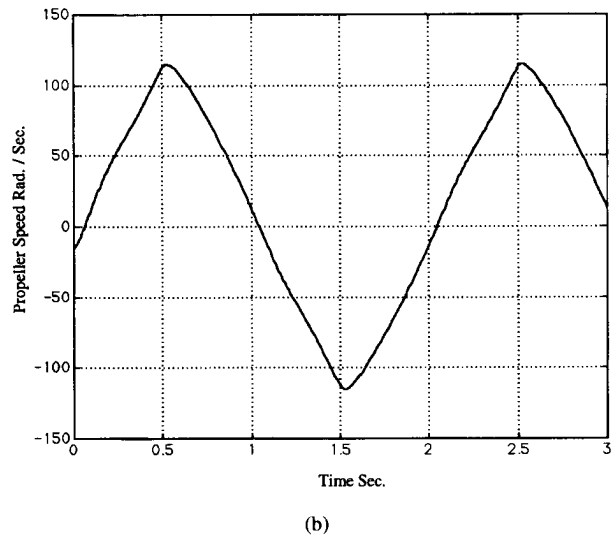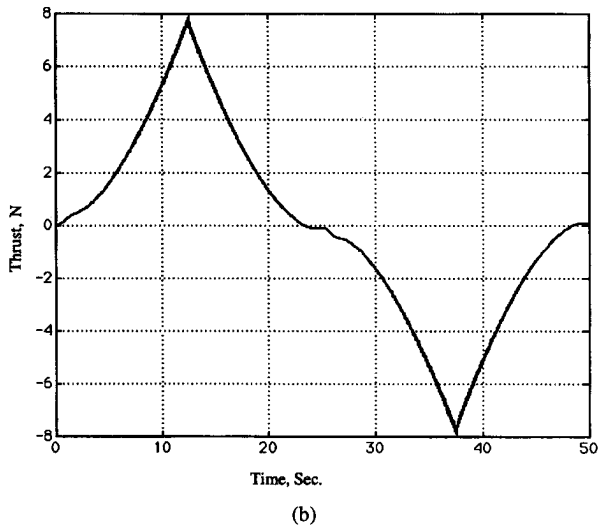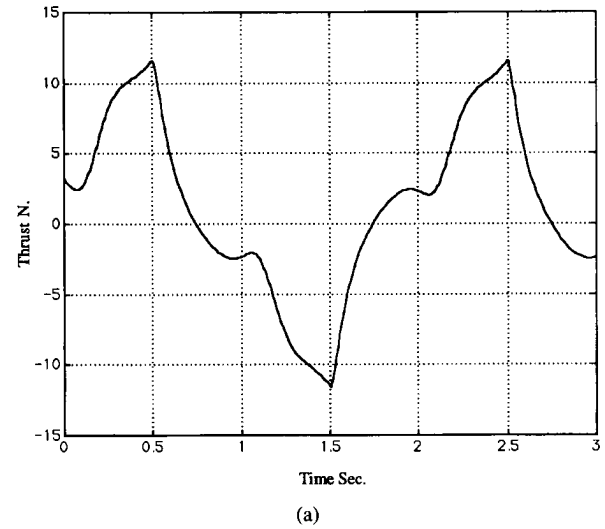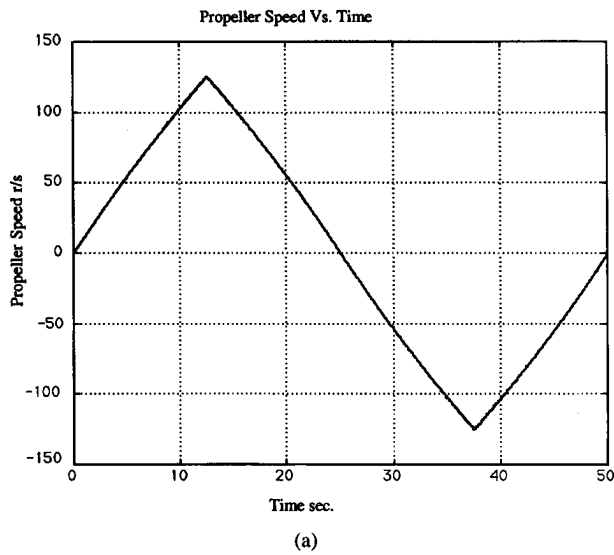
(a)

(b)

Fig. 7. (a) Propeller speed (rad/s) versus time (s). (b) Thrust (N) versus time (s).
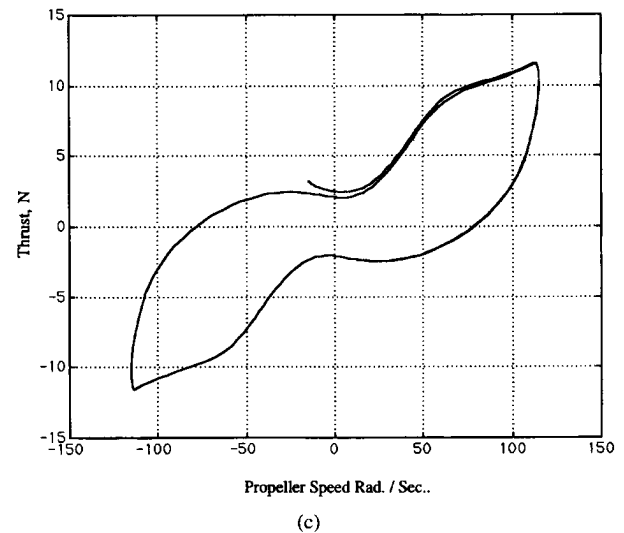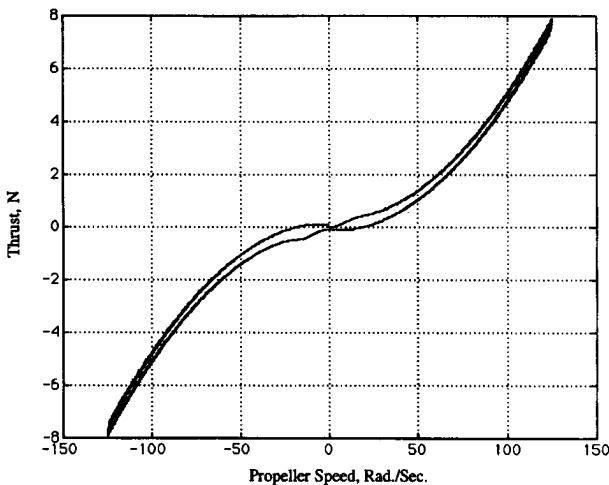

Fig. 8. Steady-state map of thrust (N) versus propeller speed (rad/s).

B. Short Period Triangular Wave Inputs

Fig. 9 (medium speed triangular) shows that as the input wave period is shortened, the influence of the inertial response of the

(a)

(b)

(c)

Fig. 9. (a) Thrust (N) versus time (s) two-second period triangular wave input. (b) Propeller speed (rad/s) versus time (s). Two-second period triangular wave input. (c) Two-second period triangular wave input thrust (N) versus propeller speed (rad/s).

tunnel water distorts the thrust response and has in effect the trend to provide an equivalent phase lead in the thrust response or a
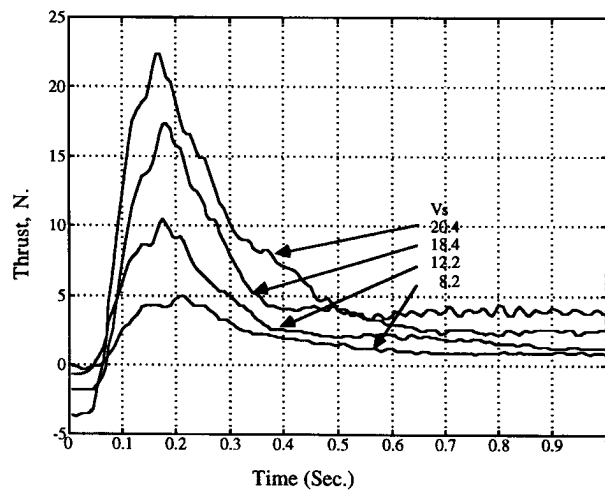
Fig. 10. Thrust force (N) versus time (s) for tunnel thruster with 30° blade and tunnel length $L/D = 6$, various input voltage levels.

Fig. 12. Model thrust (N) compared with experimental data for 50-s period triangular wave inputs of voltage.
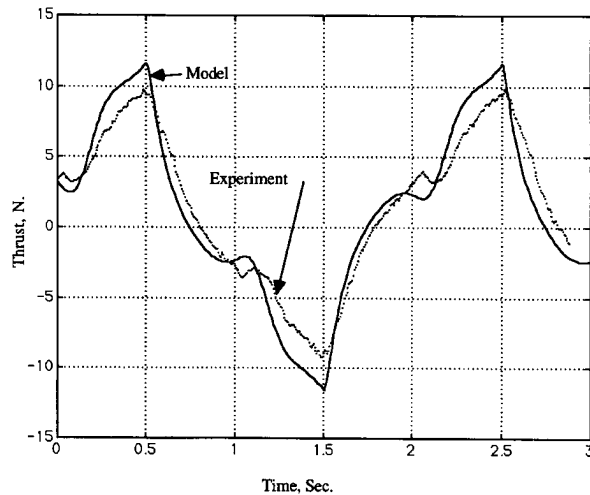

Fig. 11. Model thrust (N) compared with experimental data for 2-s period triangular wave inputs of voltage.

response component that is more allied to the acceleration of the propeller—shown nicely for triangular waves as the slope of the input.

C. Step Input Effects of Amplitude

In this experimental series the amplitude of a square wave input at 2-s period was varied and the thrust response studied. What is interesting is that both the steady state and transient peak thrust are dependent on the square of the input magnitude rather than the steady state values only.

VII. PARAMETER IDENTIFICATION AND MODEL VALIDATION

The model was matched to one particular set of data then compared to others for validation. The set used to identify the four parameters above was the 2-s period square wave with the maximum 20.4 V input level. The two disposable parameters $\Delta\beta$ and γ are usually limited in range, while the lift and drag coefficients are generally less than 2. Application of engineering heuristics, leads to the notion that increasing the lift coefficient gives a larger model peak maximum thrust for the input condition; increasing the drag coefficient increases the blade loading and hence reduces the motor steady state speed
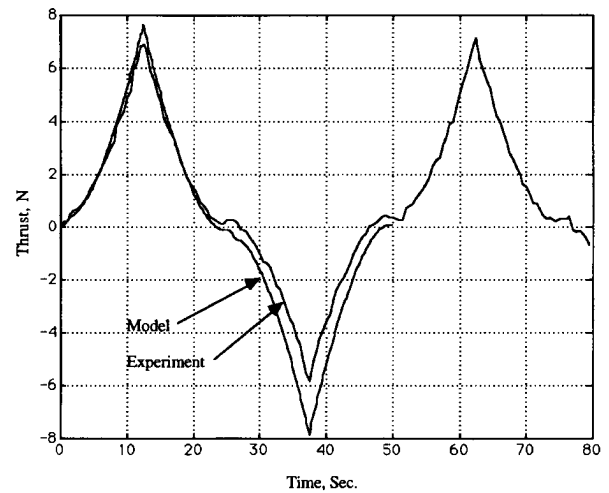
for the same voltage input; increasing the added mass coefficient γ, affects the transient response overshoot time constant; and increasing $\Delta\beta$, increases the steady state thrust at a given steady state motor speed. The final data set is given as

$$C_{L\,max} = 1.75$$
$$C_{D\,max} = 1.2$$
$$\gamma = 0.5$$
$$\Delta\beta = 0.2.$$

while the values of the motor constants taken from manufacturers data are given to yield the final parameters of the model for the tunnel thruster to be,

$$K_1 = 70.15$$
$$K_2 = 1133.2$$
$$K_h = 17\,790$$
$$K_3 = 0.954$$
$$K_4 = 0.910.$$

The series of Figs. 11–13 show the validity of the model for predicting consistent results through triangular and step type inputs. One common point about all data is the asymmetry between forward and reverse motion. Symmetry is a strong function of the blade shape and thruster design and is reflected in the model in terms of effective lift/drag map used. In our case, we have a symmetric mapping and attempted only to match positive going thrust in the first 2 quadrants. A slight modification to the map for third quadrant operation would model the reverse direction thrust better, but is not presented here.

VIII. OPEN-BLADED THRUSTER TESTS

The test apparatus and approach used for the open-bladed unit was similar to that used in the tunnel thruster tests described above. The principal difference was that the propeller used (15-cm diameter) was much lower solidity and the duct was short (10 cm). Other differences included a different drive motor (variable reluctance) that was current driven rather than voltage driven. It had a maximum torque of 0.65 Nm. This configuration is typical of the thrusters incorporated in the OTTER research vehicle developed at the Monterey Bay Aquarium Research Institute. Details of the test apparatus in Fig. 6 are presented in [4] and [5].
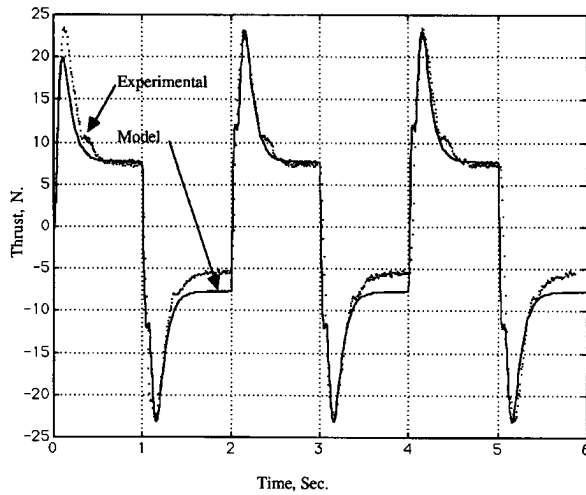
Fig. 13. Model compared with experimental thrust (N) data for square wave inputs of voltage.

Fig. 14. Model compared with experimental motor speed data for square wave inputs of voltage.

A. Parameter Identification and Model Validation

The form of the model used to describe the open-bladed thruster was identical to that used for the tunnel thruster and is described in Fig. 5. The difference is in the choice of specific parameter values.

A set of parameter values characteristic of this open-bladed thruster configuration was determined using a least-squares identification approach with selected sets of experimental test data. The results of this analysis yielded

$$C_{L\,\text{max}} = 2$$
$$C_{D\,\text{max}} = 0.5$$
$$\gamma = 2.26$$
$$\Delta\beta = 1.7.$$

In addition, because this configuration is open-bladed, a time constant was found to be $\tau = 1/90$ s.

The motor parameters were

$$K_1 = 10.8$$
$$K_h = 8333$$
$$K_2 = 0.65$$
$$K_3 = 4.0$$
$$K_4 = 30.0.$$

If these values are compared with those generated for the tunnel thruster, several points are of interest. First, the results for the motor show a significantly lower value of K_1. The reason for this is that since the motor in this configuration is current driven, the back EMF contribution to K_1 is eliminated. In fact, for the open-bladed tests, K_1 was augmented with small stiction and quadratic terms to represent the effects of the shaft seal and the effects of moving parts in the oil filled encoder attached to the motor.

The values of $C_{L\,\text{max}}$ and $C_{D\,\text{max}}$ are comparable, but indicate the reduction in drag that is associated with a lower solidity propeller.

Also of interest is that the effective change in duct length (i.e. apparent mass of the accelerated water column), γ, and the differential steady momentum flux coefficient, $\Delta\beta$, are significantly larger for the open bladed configuration than for the tunnel configuration.

A value of the time constant of 1/90 s was found to be required to explain the effects on thrust buildup due to the conversion of angular to linear momentum.
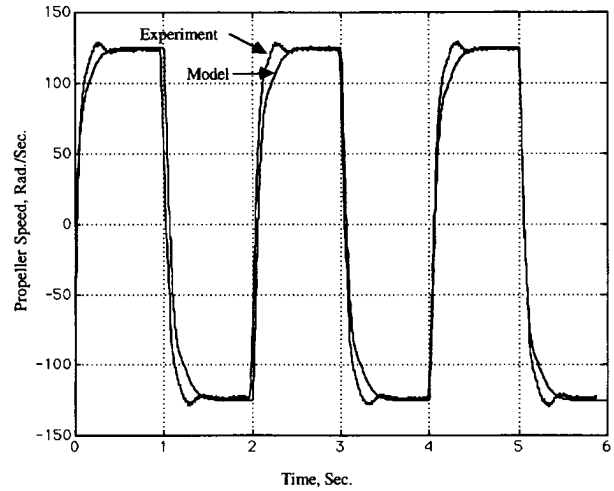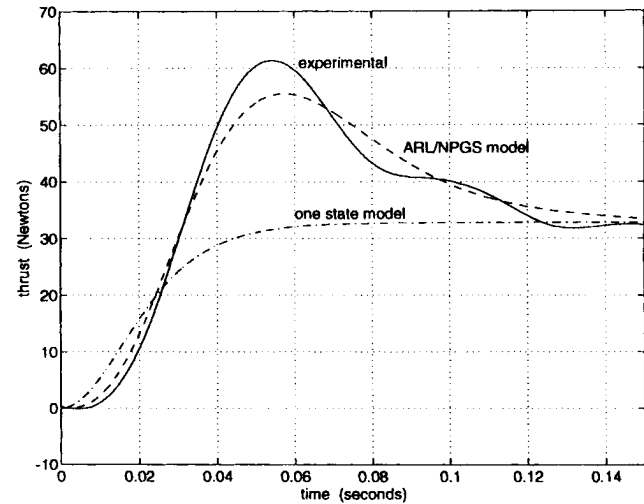

Fig. 15. Comparison of models for step input with experimental thrust.

B. Results

The steady-state testing done with the open-bladed configuration generally supported the same conclusions as reported in the tunnel thruster tests reported above, and therefore will not be reported here. Instead, the results of the open-bladed testing for step inputs will be stressed since they explain clearly the benefits of a two-state model over a single-state model in predicting the thrust transient time history.

A typical response to a step in motor input current is presented in Fig. 15.

Shown in the figure are three time histories of thrust. The first is experimental data, the second is the response predicted by a one-state model, and the third is the response predicted by the new two-state model. The form of the one-state model is consistent with that reported in Yoerger et al. [1]. The specific form used was

$$\dot{\omega}_m = Q_\text{in}/I - C_D\omega_m^2$$
$$T = K_5\omega_m^2.$$

Note that the same values of input torque and motor inertia used in the two state model were used for the one-state model. The value of C_D was adjusted to match the correct steady-state propeller velocity. The value of K_5 was adjusted to match the steady-state thrust.

The major conclusion which can be drawn from the data of Fig. 15 is that the two-state model is able to exhibit the overshoot in thrust that is typical of the experimental data whereas the one-state model is unable to explain this behavior. This result is consistent with the results presented above for the tunnel thruster unit (see Figs. 13 and 14).

Another conclusion is that the form of the generic thruster model presented in Fig. 5 works well for the two very different thruster configurations considered in this study.

IX. CONCLUSION

We believe that the approach presented here gives the structure of a thruster model that can be used to model all units in ROV/AUV applications. Specifically the model addresses transient response through four quadrants of operation and is based in the coupling of a blade mapping function to a motor and a fluid dynamics component. Further, since recently developed motors can be highly responsive, transient response to rapid stepwise inputs shows a tendency for a thrust overshoot to occur resulting from fluid inertial effects as rapid blade action reacts with the surrounding fluid medium.

The identification of key parameters for a particular blade map can be accomplished from a few simple transient response tests, and we have found the test stand described to be a convenient tool for this purpose. Finally, the model will be useful for the development of more advanced motor and thrust control schemes requiring model based control techniques.

APPENDIX

(See [6].)

$$A = 0.00445 \, \text{m}^2$$

$$D = 0.0762 \, \text{m}$$

$$L = 0.4191 \, \text{m}$$

$$J_m = 1.63e\text{-}5 \, \text{kg m}^2$$

$$J_p = 3.448e\text{-}5 \, \text{kg m}^2$$

$$C_p = 0.00022$$

$$C_p = 0.0$$

$$R = 1.73 \, \text{ohms}$$

$$K_m = 0.055 \, \text{voltsec/rad}$$

$$K_t = 0.0551 \, \text{Nm/amp}$$

$$N = 2$$

$$\rho = 998 \, \text{kg/m}^3.$$

REFERENCES

[1] D. R. Yoerger, J. G. Cooke, and J. J. E. Slotine, "The influence of thruster dynamics on underwater vehicle behavior and their incorporation into control system design," *IEEE J. Oceanic Eng.*, vol. 15, no. 3, pp. 167–178, 1991.

[2] M. B. McLean, "Dynamic performance of small diameter tunnel thrusters," MSME thesis, Naval Postgraduate School, Monterey, CA, Mar. 1991.

[3] S. E. Cody, "An experimental study of the response of small thrusters to step and triangular wave inputs," MSME thesis, Naval Postgraduate School, Monterey, CA, Dec. 1992.

[4] D. Miles, D. Burton, M. Lee, and S. M. Rock, "Closed loop force control of an underwater thruster," Monterey Bay Aquarium Research Institute/Stanford Aerospace Robotics Laboratory Internal Report, Oct. 1992.

[5] J. C. Adams, D. Burton, and M. Lee, "Dynamic characterization and control of thrusters for underwater vehicles," Monterey Bay Aquarium Research Institute/Stanford Aerospace Robotics Laboratory Internal Report, Sept. 1991.

[6] J. P. Brown, "Four quadrant model of the NPS AUV II thruster," MSME thesis, Naval Postgraduate School, Monterey, CA, Sept. 1993.

[7] E. V. Lewis, "Principles of naval architecture," *Soc. Naval Architects, Marine Eng.*, vols. 1–3, 1988.

[8] L. Prandtl and A. Betz, "Vier abhandlungen zur hydrodynamik und aerodynamik," Gottingen, 1927.

[9] E. V. Lewis, "Principles of naval architecture," *Soc. Naval Architects, Marine Eng.*, vol. II, pp. 144–145, 1988.

[10] T. I. Fossen, "Nonlinear modeling and control of underwater vehicles," Dr.Ing. thesis, Norwegian Institute of Technology, Trondheim, 1991.

[11] S. I. Sagatun, "Modeling and control of underwater vehicles: A Lagrangian approach," Ph.D. dissertation, Norwegian Institute of Technology, Trondheim, 1992.

[12] W. P. A. Van Lammeren, J. D. Van Manen, and M. W. C. Oosterveld, "The Wageningen B-screw series," *Trans. SNAME*, pp. 269–317, Nov. 1969.

[13] M. A. Rickards, "Cycloidal propulsion of submersibles," *J. Hydronautics*, vol. 4, no. 2, pp. 66–72, Apr. 1970.

[14] F. M. White, *Fluid Mechanics*, 2nd ed. New York: McGraw Hill, 1986, p. 142.

Advances in the State of the Art for AUV Inertial Sensors and Navigation Systems

R. Cox and S. Wei

Abstract—Inertial navigation reference units are often thought of as simply a navigation device which must be augmented by another device to damp the Schuler oscillation and characteristic long-term drift. Emerging applications of AUV's, however, demonstrate a need for increasingly sophisticated inertial sensors. These inertial sensors are used not only for navigation, but as importantly, they provide data for sensor stabilization.

Inertial systems have also traditionally represented a significant hotel load, been heavy, bulky, and a source of acoustic and structure-borne noise. This paper presents an overview of two new inertial systems that are now in production at the Guidance and Control Systems Division of Litton Systems, Inc. These units are small, lightweight, require little power, and are silent.

Data are presented that show long-term performance as well as short-term attitude, position, and velocity reference data for the LN-100 system. Attitude, velocity, and body axis rate data are required for stabilization of such devices as laser line scanners and long baseline side-scan sonars. The relationship between the characteristics of these sensors and inertial type errors is explored. This analysis shows that it is not sufficient to specify the inertial system only in terms of its navigation CEP. The specification of the inertial unit must also be based on the needs of the sensor payload and include such considerations as short-term stability, the noise content, phase, and bandwidth of the stabilization reference.

I. INTRODUCTION

An autonomous underwater vehicle (AUV) can be used for both military and commercial applications. Military applications include,